Luminescent Properties in Relation to Controllable Phase and Morphology of LuBO$_3$:Eu^{3+} Nano/Microcrystals Synthesized by Hydrothermal Approach

Yanping Li,[†,‡] Jiahua Zhang,*,[†] Xia Zhang,[†] Yongshi Luo,[†] Shaozhe Lu,[†] Xinguang Ren,[†] Xiaojun Wang,[†,§] Lingdong Sun,[||] and Chunhua Yan[||]

Key Laboratory of Excited State Processes, Changchun Institute of Optics, Fine Mechanics and Physics, Chinese Academy of Sciences, 16 Eastern South Lake Road, Changchun 130033, China, Graduate School of Chinese Academy of Sciences, Beijing 100039, China, Department of Physics, Georgia Southern University, Statesboro, Georgia 30460, and State Key Laboratory of Rare Earth Materials Chemistry and Applications, PKU-HKU Joint Laboratory on Rare Earth Materials and Bioinorganic Chemistry, Peking University, Beijing 100871, China

The calcite and vaterite type LuBO$_3$:Eu^{3+} nano/microcrystals with various morphologies were synthesized by the hydrothermal (HT) approach through controlling the pH values of the precursor solutions. The calcite type LuBO$_3$:Eu^{3+} shows the dominant magnetic dipole $^5D_0-^7F_1$ emission due to S_6 inversion symmetry of Lu. It also shows a symmetrical O−Eu charge transfer (CT) excitation band, which, however, is asymmetrical and broad in the material prepared by the solid-state (SS) reaction method. The effect of the residual OH$^-$ groups introduced in HT synthesis is discussed on O−Lu exciton annihilation and local environment distortion. Two different Eu^{3+} centers, one of which is with inversion symmetry, are observed in vaterite type LuBO$_3$:Eu^{3+}. The HT sample with nanostructures, such as vaterite type flowerlike LuBO$_3$:Eu^{3+}, demonstrates a red shift of the CT band and appearance of a long excitation tail at the long wavelength side of the CT band. XRD, selective excitation and fluorescence decay measurements indicate that the red shift is induced by an increase of crystal lattice parameters, and the excitation tail is responsible to the Eu^{3+} ions located at lower symmetric sites. These sites are attributed to the positions at or close to the surface of the nanostructures in the sample. As the lower symmetric sites are selectively excited, the red emission of $^5D_0-^7F_2$ of Eu^{3+} enhanced twice relatively to the orange emission of $^5D_0-^7F_1$, exhibiting superior color chromaticity in red for display application. The luminescence properties of interior Eu^{3+} and outside Eu^{3+} are studied and discussed in detail.

1. Introduction

Rare earth orthoborates LnBO$_3$ (Ln = La, Gd, Lu, Y, and Sc) are an important class of materials because of their high vacuum ultraviolet (VUV) transparency and exceptional optical damage thresholds. Moreover, the Eu^{3+} and Tb^{3+} doped LnBO$_3$ exhibit extraordinarily high luminescence efficiency under VUV excitation and thus are considered to be attractive candidates as VUV luminescent materials.[1,2] Among them, Eu^{3+}-doped vaterite type (Y, Gd)BO$_3$ have been applied as red emitting phosphors in the plasma display panels (PDPs) and a new generation of Hg-free fluorescent lamps.[3−5] However, their chromaticity is poor, being orange-red rather than red, for which the characteristic emissions

comprise almost equal contributions from $^5D_0-^7F_1$ and $^5D_0-^7F_2$ transitions. Consequently, considerable efforts are underway and many approaches to improve the chromaticity have been reported during the past few years.[6−8]

The LnBO$_3$ constitutes a family of polymorphous compounds with three crystalline forms of CaCO$_3$: aragonite, vaterite, and calcite, depending on the size of the cation.[9] There exists, however, no individual LnBO$_3$ with all three polymorphs. The largest rare earth ion, La^{3+}, forms an orthoborate with the orthorhombic aragonite structure. For the smaller rare earth ions, Y^{3+} and Gd^{3+}, the orthoborates possess the vaterite structure, which is consistent with a pseudohexagonal symmetry. For the smallest rare earth ion, ScBO$_3$ exhibits the rhombohedral calcite structure, having a single site for the rare earth with S_6 point symmetry. Let us note that LuBO$_3$ is a special case having two relatively stable allotropes that crystallize either with the calcite or, if heated above 1310 °C, with the vaterite structure. As a group, these

* Corresponding author. E-mail: zhangjh@ciomp.ac.cn.
† Changchun Institute of Optics, Fine Mechanics and Physics, Chinese Academy of Sciences.
‡ Graduate School of Chinese Academy of Sciences.
§ Georgia Southern University.
|| Peking University.

(1) Ren, M.; Lin, J. H.; Dong, Y.; Yang, L. Q.; Su, M. Z. *Chem. Mater.* **1999**, *11*, 1576.
(2) Tukia, M.; Hölsä, J.; Lastusaari, M.; Niittykoski, J. *Opt. Mater.* **2005**, *27*, 1516.
(3) Wang, Y. H.; Endo, T.; He, L.; Wu, C. F. *J. Cryst. Growth.* **2004**, *268*, 568.
(4) Kim, T.; Kang, S. *Mater. Res. Bull.* **2005**, *40*, 1945.
(5) Wang, L. L.; Wang, Y. H. *J. Lumin.* **2007**, *122−123*, 921.
(6) Wei, Z. G.; Sun, L. D.; Liao, C. S.; Yan, C. H. *Appl. Phys. Lett.* **2002**, *80*, 1447.
(7) Yu, Z. J.; Huang, X. W.; Zhuang, W. D.; Cui, X. Z.; Li, H. W. *J. Alloys Compd.* **2005**, *390*, 220.
(8) Pan, G. H.; Song, H. W.; Bai, X.; Liu, Z. X.; Yu, H. Q.; Di, W. H.; Li, S.; Fan, L.; Ren, X.; Lu, S. *Chem. Mater.* **2006**, *18*, 4526.
(9) Levin, E. M.; Roth, R. S.; Martin, J. B. *Am. Mineral.* **1961**, *46*, 1030.

Luminescence of LuBO₃:Eu³⁺ Crystals by HT Approach

Chem. Mater., Vol. 21, No. 3, 2009 469

orthoborates offer cation environments increasing in symmetry from aragonite to vaterite to calcite.[10-12]

As a member of rare-earth-activated LnBO$_3$, Eu^{3+}-doped LuBO$_3$ not only has been considered as an promising candidate for the aforementioned applications but also appears to be a good scintillator because of its high density.[13-15] However, in the past few years, there appeared only a few papers in the literature[10,11,14-18] concerning the preparation and luminescence properties of LuBO$_3$:Eu^{3+}. Various cation sites are observed in the vaterite type LuBO$_3$:Eu^{3+} by using luminescence probing.[11,16] It is found in rare-earth-doped orthoborates that the luminescence properties are related to the size, shape, and crystal types, which can be governed by synthetic routes and parameters.[10,19-23] So the present tendency of development of such materials is not oriented especially toward new phases but mostly toward a better knowledge and a better control of microstructures of existing materials. Nevertheless, the previously methods derived LuBO$_3$:Eu^{3+} mainly include solid-state reaction method,[10,11] sol−gel technology,[15,16] and the ammonium nitrate melt method,[17] which need high temperature or iterative grind process, leading to a bad morphology. Therefore, it is highly desired to synthesize LuBO$_3$:Eu^{3+} phosphor with homogeneous and regular morphology by a controllable approach toward durable structures. The hydrothermal (HT) approach is a good choice due to its convenience, exemption from pollution, and the possibility of achieving satisfying crystallinity at a relatively low temperature, without further calcination. Recently, Lin et al.[20] reported the preparation of vaterite type YBO$_3$:Eu^{3+} nanocrystals with flower or hedgehog fungus like shapes, utilizing direct crystallization of Y$_2$O$_3$ and Eu$_2$O$_3$ powders in H$_3$BO$_3$ solutions under acidic (pH 1−4) HT conditions.

In this paper, we report, to the best of our knowledge for the first time, on the synthesis of the calcite and vaterite type LuBO$_3$:Eu^{3+} nano/microcrystals by the HT approach at relatively low temperature around 200−220 °C. The calcite and vaterite type LuBO$_3$:Eu^{3+} with various morphologies composed of nanoscaled structures have been obtained by adjusting the pH values of the mixed solutions of Lu(NO$_3$)$_3$, Eu(NO$_3$)$_3$, and H$_3$BO$_3$ in the range of 7−9. Two cation sites are observed in the vaterite type sample. The unique luminescence properties of the nanoscaled structures are studied in detail. The enhanced red emission relative to the orange one is performed, demonstrating improvement of the chromaticity in red. For comparison, we also prepared identically doped LuBO$_3$:Eu^{3+} bulk powders using traditional solid-state reaction method.

2. Experimental Section

2.1. Sample Preparation. The synthesis of LuBO$_3$:Eu^{3+} samples via the hydrothermal approach can be described as follows: appropriate amounts of high-purity Lu$_2$O$_3$ and Eu$_2$O$_3$ powders were dissolved in dilute HNO$_3$, respectively, to form Lu(NO$_3$)$_3$ and Eu(NO$_3$)$_3$ solutions. A slight excess of HBO$_3$ was added into an appropriate amount of Lu(Eu)(NO$_3$)$_3$ solution under magnetic stirring to form a homogeneous solution at room temperature. Then the pH was adjusted to a specific value by adding dropwise dilute NH$_3$·H$_2$O solution. After continuous stirring for 2 h, the milky colloidal solution was transferred into a closed Teflon-lined stainless steel autoclave with 50.0 mL capacity, and subsequently heated at a temperature in the range of 200−220 °C for 5−12 h. As the autoclave cooled to room temperature, the resultant products were obtained by filtering, washing with deionized water several times, and drying at 65 °C in a vacuum oven.

For comparison, we also prepared the calcite and vaterite type LuBO$_3$:Eu^{3+} bulk powders by traditional solid-state (SS) reaction method, at sintering temperatures of 1000 and 1400 °C for 3 h, respectively, using starting materials of Lu$_2$O$_3$, Eu$_2$O$_3$, and HBO$_3$.

2.2. Measurements and Characterization. The crystalline structure of all samples were characterized by X-ray diffraction (XRD) (Rigaku D/max-rA power diffractometer using Cu Kα (λ = 1.54178 Å) radiation). Field emission scanning electron microscopy (FE-SEM) images were taken on S-4800 (Hitachi Company) electron microscopes. The emission and excitation spectra were measured with a Hitachi F-4500 spectrophotometer equipped with a continuous 150W Xe-arc lamp. For comparison of different samples, the spectra were measured with the same instrument parameters (2.5 nm for the excitation slit, 1.0 nm for the emission slit, and 700 V for the PMT voltage). In lifetime measurements, the fourth (266 nm) harmonic of a Nd:YAG laser (spectra-physics, GCR 130) and 468 nm light pulse from an optical parametric oscillator were used as excitation sources, and the signals were detected with a Tektronix digital oscilloscope model (TDS 3052).

3. Results and Discussion

3.1. Morphology and Crystal Structure Control. In the HT synthetic process, we find the pH value of the precursor solution has a crucial effect on the formation of phase type and morphology of LuBO$_3$:Eu^{3+} sample, as the FE-SEM images illustrated in Figure 1. When the pH is adjusted to be 7, a pure calcite type LuBO$_3$:Eu^{3+} with the morphology in a form of diamond is formed, as shown in Figure 1A. However, no product can be obtained if the pH is below 7. With gradually increasing the pH from 7 up to 8.7, additional morphology in a form of microclewlike appears and increases continuously in number, while the number of the originally diamond shaped morphology decreases. The numbers of the two kinds of morphologies are nearly equal as the pH is 8, as illustrated in Figure 1B. As the pH reaches to 8.7, only

(10) Avella, F. J.; Sovers, O. J.; Wiggins, C. S. *J. Electrochem. Soc.: Solid State Sci.* **1967**, *114*, 613.

(11) Hölsä, J. *Inorg. Chim. Acta* **1987**, *139*, 257.

(12) Chadeyron, G.; El-Ghozzi, M.; Mahiou, R.; Arbus, A.; Cousseins, J. C. *J. Solid State Chem.* **1997**, *128*, 261.

(13) Boyer, D.; Leroux, F.; Bertrand, G.; Mahiou, R. *J. Non-Cryst. Solids* **2002**, *306*, 110.

(14) Bertrand-Chadeyron, G.; Boyer, D.; Dujardin, C.; Mansuy, C.; Mahiou, R. *Nuclear Instrum. Methods Phys. Res., Sect. B* **2005**, *229*, 232.

(15) Mansuy, C.; Nedelec, J. M.; Dujardin, C.; Mahiou, R. *Opt. Mater.* **2007**, *29*, 697.

(16) Boyer, D.; Bertrand-Chadeyron, G.; Mahiou, R.; Lou, L.; Brioude, A.; Mugnier, J. *Opt. Mater.* **2001**, *16*, 21.

(17) Klassen, N. V.; Shmurak, S. Z.; Shmytko, I. M.; Strukova, G. K.; Derenzo, S. E.; Weber, M. J. *Nuclear Instrum. Methods Phys. Res., Sect. A* **2005**, *537*, 144.

(18) Mansuy, C.; Tomasella, E.; Mahiou, R.; Gengembre, L.; Grimblot, J.; Nedelec, J. M. *Thin Solid Films* **2006**, *515*, 666.

(19) Wang, Y. H.; Uheda, K.; Takizawa, H.; Endo, T. *Chem. Lett.* **2001**, *3*, 206.

(20) Zhang, J.; Lin, J. *J. Cryst. Growth* **2004**, *271*, 207.

(21) Jiang, X. C.; Sun, L. D.; Yan, C. H. *J. Phys. Chem. B* **2004**, *108*, 3387.

(22) Lin, C. K.; Kong, D. Y.; Liu, X. M.; Wang, H.; Yu, M.; Lin, J. *Inorg. Chem.* **2007**, *46*, 2674.

(23) Pan, G. H.; Song, H. W.; Yu, L. X.; Liu, Z. X.; Bai, X.; Lei, Y. Q; Fan, L. B. *J. Lumin.* **2007**, *122−123*, 882.
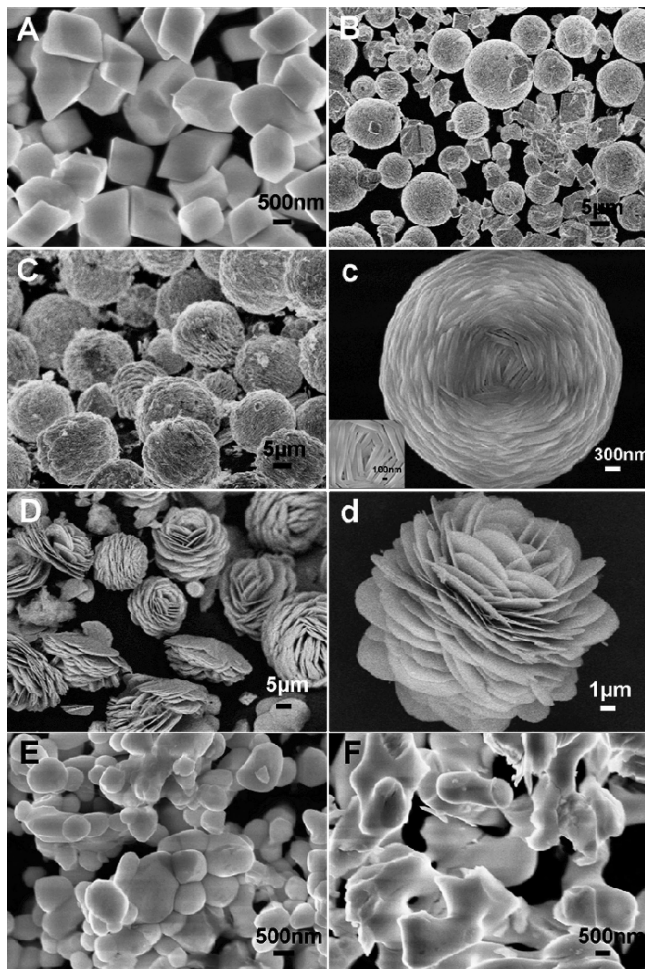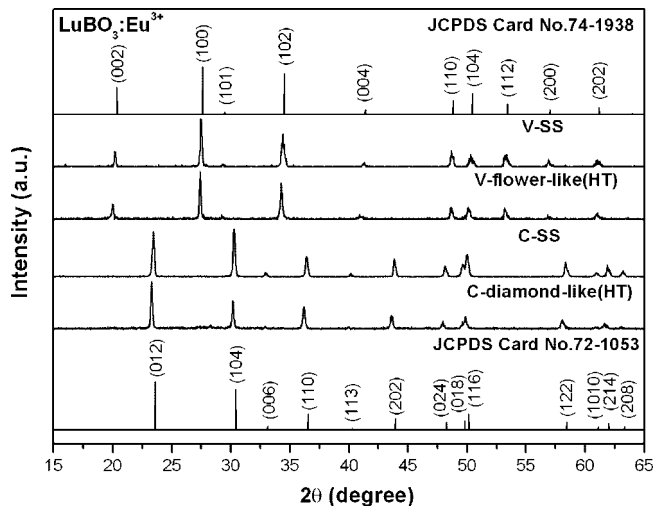
Figure 1. (A−D) FE-SEM images of LuBO$_3$:Eu^{3+} samples prepared by HT, corresponding to pH 7, 8, 8.7, and 9, respectively (c, d) Enlarged images of C and D, respectively. (E, F) Images of LuBO$_3$:Eu^{3+} bulk powders prepared by SS, corresponding to the calcite and vaterite type, respectively.

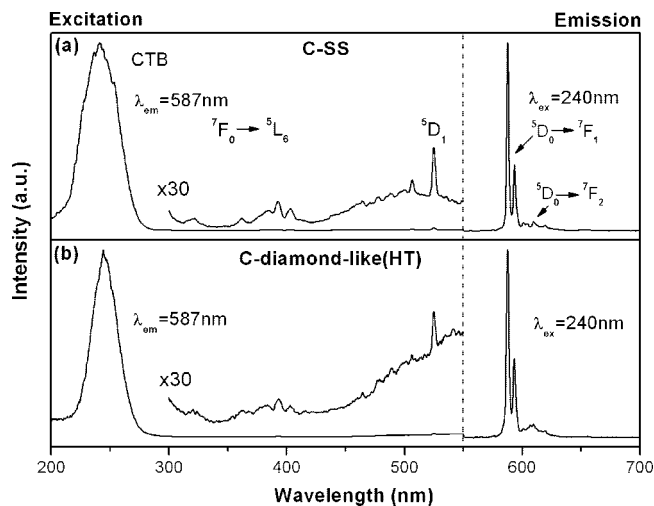**Figure 2.** XRD patterns of LuBO$_3$:Eu^{3+} samples.

V-flower-like(HT), respectively. Different from C-diamond-like(HT) sample, both V-clew-like(HT) and V-flower-like(HT) samples have nanoscaled substructures with them. Each clew in the V-clew-like(HT) sample has a diameter of 20 μm and is intertwined by nanoscaled bands with the width of ~100 nm (see Figure 1c). Similarly, each flower in the V-flower-like(HT) sample is with the diameter of 10 μm, and is composed of packed nanoscaled leaves with the thickness of ~100 nm (see Figure 1d).

Images E and F in Figure 1 show the FE-SEM images of the calcite type LuBO$_3$:2% Eu^{3+} and vaterite type LuBO$_3$: 0.6% Eu^{3+} bulk powders, which are prepared by SS, and labeled as C-SS and V-SS, respectively. The morphology of sample C-SS is close to a ball with diameter less than 1.5 μm and sample V-SS is very abnormal, showing that HT is more beneficial for gaining dispersible and regular products against the SS.

Figure 2 shows the XRD patterns of four samples: C-diamond-like(HT), C-SS, V-flower-like(HT), and V-SS. The XRD patterns demonstrate that the C-diamond-like(HT) and C-SS sample belong to the trigonal system LuBO$_3$ with calcite type (JCPDS No.72−1053), and the V-flower-like(HT) and V-SS sample belong to the hexagonal system LuBO$_3$ with vaterite type (JCPDS No. 74−1938). The C-diamond-like(HT) and V-flower-like(HT) samples are on the scale of micrometers. The substructure in V-flower-like(HT) is in the scale of ~100 nm, not small enough to broaden the XRD peaks of the HT samples. It is clearly exhibited that the XRD peaks of V-flower-like(HT) shift to the smaller angle side in comparison with the V-SS sample, indicating an increase in lattice parameters in the V-flower-like(HT) sample. The lattice parameters of the two samples are calculated from XRD patterns: $a = 3.7476$ Å, $c = 8.7484$ Å in the V-SS sample and $a = 3.7592$Å, $c = 8.7779$Å in the V-flower-like(HT) sample.
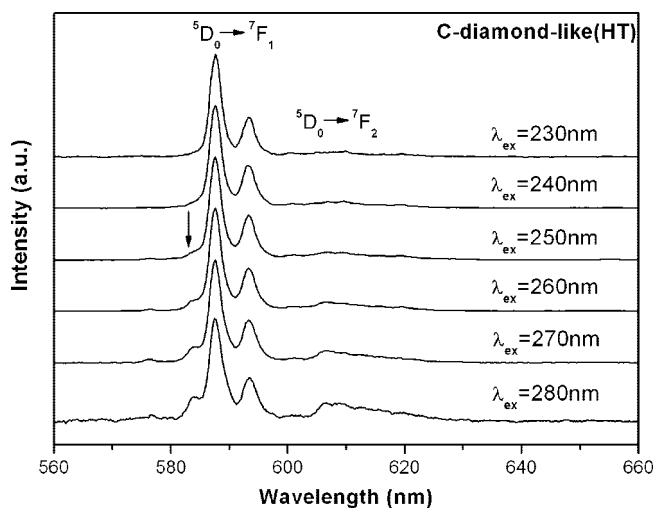
3.2. Luminescence Poperties of C-SS and C-Diamond-Like(HT) LuBO$_3$:Eu^{3+}. Figure 3 shows the emission and excitation spectra of sample (a) C-SS and (b) C-diamond-like(HT). Because of Eu^{3+} substituting for Lu^{3+} site with inversion S_6 symmetry in calcite type LuBO$_3$, the electric dipole transitions, i.e., the $^5D_0-^7F_2$ transition, are in

microclewlike product remains, as shown in Figure 1C,c. The microclewlike products are characterized to be pure vaterite type LuBO$_3$:Eu^{3+} by XRD and spectroscopic analysis. If the pH is further increased from 8.7, the microclewlike products gradually change their shapes to be microflowerlike but without crystal phase transformation. The morphology of the product is completely in the form of microflowerlike as pH reaches 9, as shown in Figure 1D,d.

In the HT synthesis process, we found the formation of pure calcite type LuBO$_3$:Eu^{3+} requires Eu^{3+} concentration higher than 2 mol %. In the SS synthesis process, we found undoped LuBO$_3$ cannot form pure vaterite type. As the Eu^{3+} concentration is higher than 0.6 mol %, pure vaterite type LuBO$_3$:Eu^{3+} can be obtained. Therefore, the Eu^{3+} concentrations of 2 mol % for calcite type and 0.6 mol % for vaterite type are selected in this work for comparably investigating the luminescence properties of the materials prepared by the HT and SS methods.

The calcite type LuBO$_3$:2% Eu^{3+} sample in the shape of a diamond is synthesized at 200 °C for 5 h by HT. We label it as C-diamond-like(HT). It is with a uniform size of about 1.5 μm (see Figure 1A). The vaterite type LuBO$_3$:0.6% Eu^{3+} in the shape of either clew or flower is synthesized at 220 °C for 12 h by HT. We label them as V-clew-like(HT) and

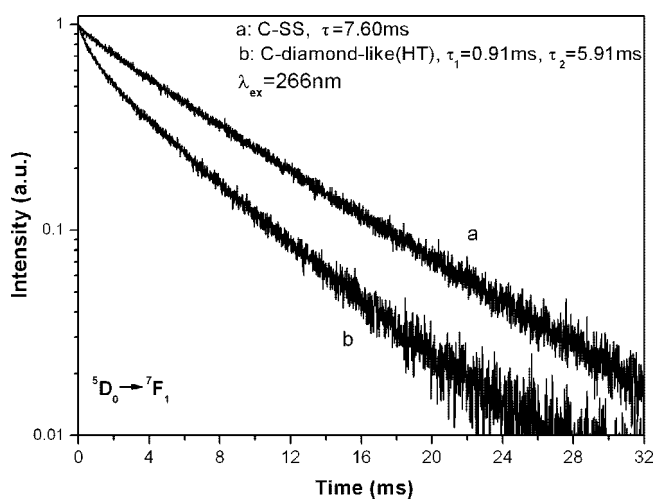**Figure 3.** Excitation spectra and emission spectra of calcite type LuBO₃: Eu³⁺ for (a) sample C-SS and (b) sample C-diamond-like(HT).

principle forbidden and the magnetic dipole transition $^5D_0-^7F_1$, therefore dominates the emission, as reported by Hölsä.[11] The $^5D_0-^7F_1$ emission contains only two lines, located at 587 and 593nm, respectively, indicating the $^7F_1$ is split into two sublevels in calcite type LuBO₃ crystal field. It is also observed in the emission spectra that a very weak emission at 610 nm, originating from $^5D_0-^7F_2$ of Eu³⁺, appears, implying that a little bit of Eu³⁺ ions occupy sites with lower symmetry deviated from S_6 to allow electric dipole transition. In the excitation spectra, the f−f excitation is dominated by the magnetic dipole transition of $^7F_0-^5D_1$ at 525 nm with a weak $^7F_0-^5L_6$ peak at 395 nm, further reflecting the effect of Eu³⁺ with inversion symmetry. There appears a strong band located at 240 nm in the excitation spectra. This band is well-known to attributed to $O^{2-}-Eu^{3+}$ charge transfer band (CTB)[24] from the 2p orbital of O^{2-} to the 4f orbital of Eu³⁺. An obvious difference in the spectra between the two samples appears in their CTBs. It can be seen that the wing at the high energy side of the CTB in C-SS sample is stronger than that in C-diamond-like(HT) sample, leading to a asymmetrical and broad CTB in C-SS against the C-diamond-like(HT). As the results in YBO₃: Eu³⁺ [24] and Y₂O₃:Eu³⁺,[25] there is a O−Y excitonic absorption band in the range of 200~220 nm. It is thus speculated that the CTB in C-SS sample contains the contribution from O−Lu excitonic absorption, which is able to effectively transfer energy to Eu³⁺. In C-diamond-like(HT), however, the energy transfer from O−Lu exciton to Eu³⁺ is ceased, leading to undetectable O−Lu excitonic excitation band and thus a narrow and symmetrical pure CTB left. The exciton annihilation is perhaps performed by many residual OH⁻ groups with a large vibration frequency introduced in HT synthesis at low temperature. These groups may also distort the local crystal structures. One of the evidence for that is the $^5D_0-^7F_2$ electric dipole emission in C-diamond-like(HT) is slightly stronger than that in C-SS sample, as shown in Figure 3.

(24) Wei, Z. G; Sun, L. D.; Liao, C. S.; Jiang, X. C.; Yan, C. H.; Tao, Y.; Hou, X. Y.; Ju, X. *J. Appl. Phys.* **2003**, *93*, 9783.
(25) Jia, M. L.; Zhang, J, H.; Lu, S. Z.; Sun, J. T.; Luo, Y. S.; Ren, X. G.; Song, H. W.; Wang, X *J. Chem. Phys. Lett.* **2004**, *384*, 193.

Figure 4. Emission spectra of the sample C-diamond-like(HT) LuBO₃:Eu³⁺ under excitation at various wavelengths of CTB.
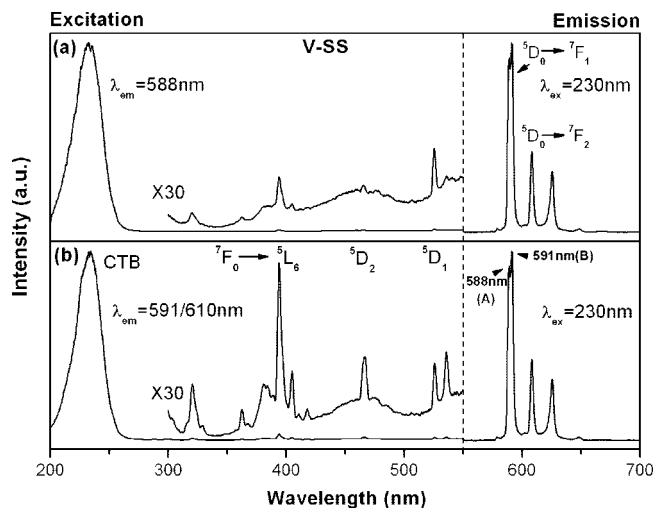

Figure 5. Fluorescence decay curves of $^5D_0-^7F_1$ transition of calcite type LuBO₃:Eu³⁺ samples.

To further confirm the distorted local crystal structure in C-diamond-like(HT) sample, emission spectra are measured under excitation at various wavelengths within its CTB from 230−280 nm, as shown in Figure 4. One can find the third line of the $^5D_0-^7F_1$ emission appears at 584 nm, and this new line as well as the $^5D_0-^7F_2$ emission at 610 nm grows up with increasing excitation wavelengths. The same measurement is also done in C-SS, but no obvious change is observed in the emission spectra. This measurement clearly demonstrates the distorted local environment in C-diamond-like(HT) sample. The fact that the distorted local environment is favorite of longer wavelength excitation indicates that its CTB is located at the longer wavelength side of the normal environment. It is hence considered that the residual OH⁻ groups play an important role on local environment distortion in C-diamond-like(HT) LuBO₃:Eu³⁺.

Figure 5 shows the fluorescence decay curves for the $^5D_0-^7F_1$ transition in C-SS and C-diamond-like(HT) LuBO₃: Eu³⁺ excited by a 266 nm nanosecond-pulsed laser. The decay in C-SS exhibits a single exponential function with a lifetime of 7.60 ms, which is expectably more longer than that (2.75 ms) in vaterite type V-SS sample because of

Figure 6. Excitation spectra (a) λ_{em} = 588nm, (b) λ_{em} = 591/610 nm and emission spectra (λ_{ex} = 230nm) of sample V-SS.

Figure 7. Emission spectra of sample V-SS $LuBO_3:Eu^{3+}$ excited by CTB and f−f transtions of Eu^{3+}.

magnetic dipole transition. In contrast, the decay in C-diamond-like(HT) exhibits a nonexponential function. If the decay is fitted by two exponential functions, a short lifetime of 0.91 ms and a long lifetime of 5.91 ms are induced. Considering that the allowance of the electric dipole transition in distorted environment can speed up radiative transition rate of the $^5D_0$ level, the fast and slow components may be related to the distorted and normal environments, respectively. It is noted that the slow component in C-diamond-like(HT) has a lifetime of 5.91 ms still shorter than that of 7.60 ms in C-SS sample. This is explained as the enhanced multiphonon relaxation from the $^5D_0$ level to the lower levels by assistance of the residual OH^- groups in C-diamond-like(HT) $LuBO_3:Eu^{3+}$.

3.3. Luminescence Properties of V-SS and V-Flower-Like(HT) $LuBO_3:Eu^{3+}$. Figure 6 shows the emission and excitation spectra of sample V-SS. Different from calcite type $LuBO_3$ with inversion symmetry of cation, the vaterite type rare earth orthoborates at least have two different cation sites, and most of the cations are at noninversion centers. The electric dipole transitions are no longer forbidden for most Eu^{3+} ions substituting for the cation sites. The emission spectra in V-SS sample are similar with that in vaterite type $YBO_3:Eu^{3+}$,[6,20] in which the major emissions are the $^5D_0-^7F_1$ and $^5D_0-^7F_2$ transitions. The very weak $^5D_0-^7F_0$ and $^5D_0-^7F_3$ transitions can be also observed at 580 and 650 nm, respectively. Two peaks are resolved in $^5D_0-^7F_1$ emission, located at 588 and 591 nm, respectively, as shown clearly in Figure 7. The $^5D_0-^7F_2$ emission consists a peak at 610 nm and another peak at 625 nm. The CTBs for monitoring the different emission peaks are almost identical, peaking at around 230 nm. The excitation spectra in the f−f spectral region of Eu^{3+} monitoring the 591 nm peak is consistent with that monitoring the 610 nm peak, however, is different with that monitoring the 588 nm peak, as shown in Figure 6. The excitation spectra for monitoring the 588 nm peak presents the strongest $^7F_0-^5D_1$ magnetic dipole transition at 525 nm with a very weak $^7F_0-^5D_2$ electric dipole transition at 466 nm, and that for monitoring the 591/610 nm peak exhibits the strongest $^7F_0-^5L_6$ transition at 395 nm, and a strong $^7F_0-^5D_2$ transition as well as two $^7F_0-^5D_1$
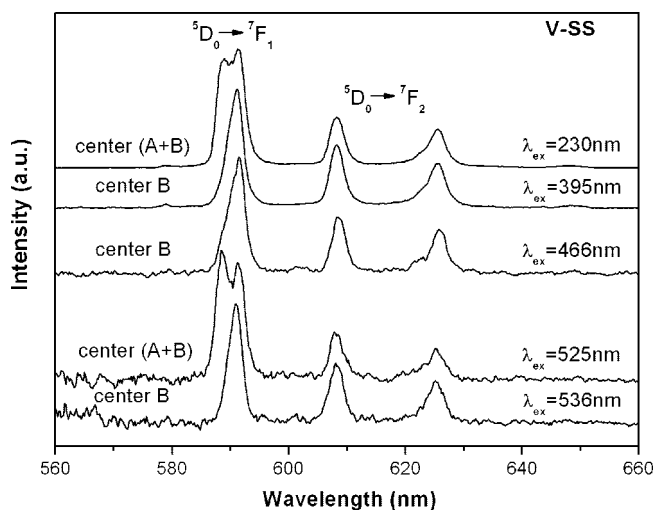
splitting lines at 525 and 536 nm, respectively. The 536 nm excitation line is absent for monitoring the 588 nm peak. This result indicates that the 588 and 591 nm emission peaks originate from two kinds of Eu^{3+} centers (denoted by center A and center B, respectively) with different point symmetries. Accordingly, emission spectra under selective excitation are performed, as shown in Figure 7. The splittings of the $^7F_1$ is only 30 cm^{-1} in vateriate type $LuBO_3:Eu^{3+}$.[11] In contrast, the energy separation of 588 and 591 nm peaks is about 86 cm^{-1}, further indicating the two peaks are not splittings of the $^7F_1$ in the same center. In comparison with the emission spectrum of vateriate type $LuBO_3:Eu^{3+}$ reported by Hölsä,[11] the 591 nm peak should consists of three $^5D_0-^7F_1$ peaks. It should be noted that the measured spectra in this work is not highly resolved as fluorescence line narrowing technique to investigate the site-selective symmetries in crystals.[26−28] The splittings of the 591 nm peak are, therefore, unfortunately unresolved in this work. As we know from Figure 6, the $^5D_0-^7F_1$ line at 591 nm and the two $^5D_0-^7F_2$ lines exhibit the identical excitation spectra, the emission of center B, hence, consists of a $^5D_0-^7F_1$ line at 591 nm and two $^5D_0-^7F_2$ lines at 610 and 625 nm. The center A should emit at 588 nm only, originating from the $^5D_0-^7F_1$ transition, without the $^5D_0-^7F_2$ emission. As a result, we can infer that center A has inversion symmetry. However, because of the low spectral resolution of the present work, the splittings of $^7F_1$ for centers A and B are not clear, and we are unable to precisely determine the symmetry of each center.

We observe experimentally that V-flower-like(HT) and V-clew-like(HT) exhibit the same luminescence properties. In this section, only V-flower-like(HT) is selected instead of V-clew-like(HT) to demonstrate its unique luminescence properties for comparing with V-SS. Figure 8 shows the emission and excitation spectra of sample V-flower-like(HT) and V-SS.

(26) Cascales, C.; Fernández, J.; Balda, R. *Opt. Express* **2005**, *13*, 2141.
(27) Cascales, C.; Balda, R.; Jubera, V.; Chaminade, J. P.; Fernández, J. *Opt. Express* **2008**, *16*, 2653.
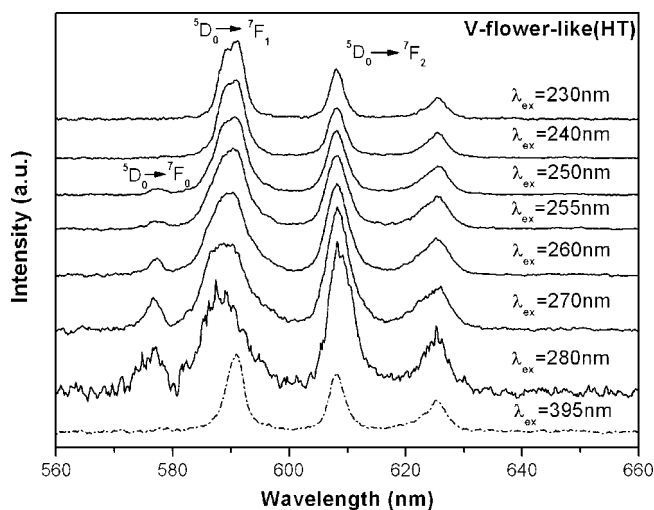(28) Gschneidner, K. A., Jr. and Eyring, L. *Handbook on the Physics and Chemistry of Rare Earths*; Elsevier Science: Amsterdam, 1996; Vol. 23, pp 121−283.
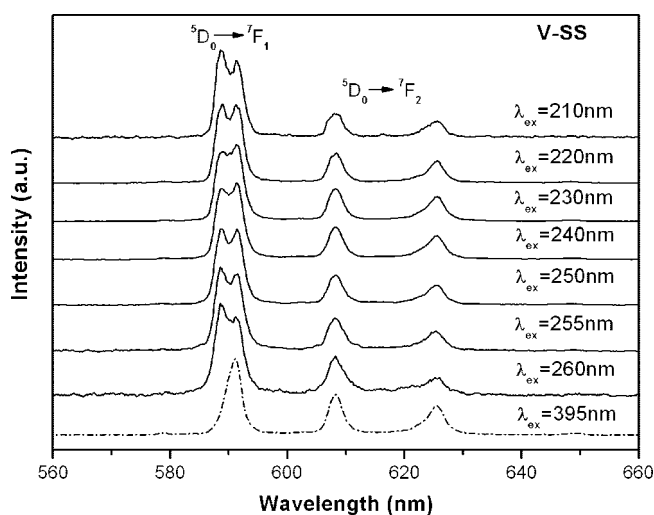
Luminescence of LuBO₃:Eu³⁺ Crystals by HT Approach

Chem. Mater., Vol. 21, No. 3, 2009 473
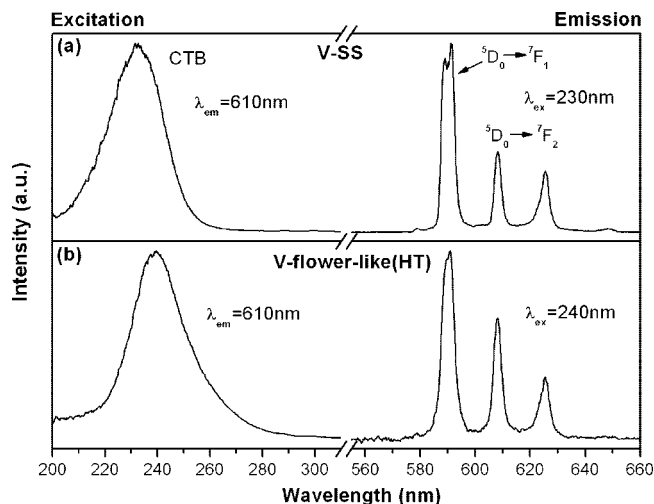
Figure 8. Excitation spectra obtained by monitoring the emission of $^5D_0-^7F_2$ and emission spectra of vaterite type $LuBO_3:Eu^{3+}$ for (a) sample V-SS and (b) sample V-flower-like(HT).

Figure 9. Emission spectra of sample V-flower-like(HT) excited by UV light at various wavelengths.

Figure 10. Emission spectra of sample V-SS excited by UV light at various wavelengths (emission intensity is normalized to the peak of the 591 nm emission line).

Comparing with V-SS, one can observe in V-flower-like(HT) that the red emission of $^5D_0-^7F_2$ is enhanced relatively to the orange emission of $^5D_0-^7F_1$, and the CTB shifts to the longer wavelength side. The enhanced red to orange intensity (R/O) ratio of Eu^{3+} implies the increase of those local environments with reduced symmetries. These lower symmetrical environments are probably induced by lots of surface positions of the nanoscaled substructures in V-flower-like(HT) sample. The red shift of O—Eu CTB in nanophosphors is often observed, such as in $Y_2O_3:Eu^{3+}$.[25,29] In the charge transfer excitation, O 2p electrons are excited into the 4f levels of Eu^{3+}, and the peak position of the CTB is determined by the energy difference between the O $2p$ valence band and the 4f levels of Eu^{3+}. As reported by Lin et al.,[30] the peak position of CTB is involved in the length of Eu—O bond: the shorter the Eu—O bond, the larger the energy difference between the 4f and O 2p electrons, and the higher energy position of the CTB. Therefore, it can be deduced from the red shift of CTB that the average Eu—O bond distance in V-flower-like(HT) sample is longer than that of sample V-SS. This explanation is well supported by the results of the XRD patterns, which demonstrates an increase in crystal lattice parameters against V-SS. Another phenomena remains in Figure 8 is that the CTB in V-flower-like(HT) shows a long tail at the long wavelength side. Accordingly, the emission spectra under excitation at various wavelengths within the CTB including its tail are measured, as shown in Figure 9.

It is found that the R/O ratio and the $^5D_0-^7F_0$ emission are all notably enhanced when the excitation wavelengths a changed from short to long. In this process, these emission lines broaden. As a result, it is inferred that more disordered environments are excited as the excitation is tuned to the longer wavelength. These disordered environments reduce the symmetries of cations and this induce more odd crystal field terms, enhancing both the $^5D_0-^7F_2$ electric dipole

transition and the $^5D_0-^7F_0$ transition. The $^5D_0-^7F_0$ transition can be resulted from admixture of 4f ^{6}5d configuration to the $4f^7$ ground configuration via the linear odd crystal field.[31,32] It is considered that these disordered environments are mainly located either near or on the surface of the nanoscaled substructures in V-flower-like(HT) sample. In this case, the Eu^{3+} ions may be classified approximately to the interior Eu^{3+} and outside Eu^{3+}. We infer that the central CTB is responsible for the interior Eu^{3+}, and the long wavelength tail of the CTB is responsible for the outside Eu^{3+} of V-flower-like(HT). It is, therefore, expected that no obvious change in emission spectra upon different excitation wavelengths can be observed in V-SS sample, as shown in Figure 10. Figure 11 shows the dependence of the R/O ratio on excitation wavelengths in V-flower-like(HT) and V-SS. The R/O ratio can increase twice in V-flower-like(HT), but remains nearly constant in V-SS.

(29) Tao, Y.; Zhao, G. W.; Zhang, W. P.; Xia, S. D. *Mater. Res. Bull.* **1997**, *32*, 501.
(30) Lin, J. H.; You, L. P.; Lu, G. X.; Yang, L. Q.; Su, M. Z. *J. Mater. Chem.* **1998**, *8*, 1051.
(31) Kiss, Z. J.; Weakliem, H. A. *Phys. Rev. Lett.* **1965**, *15*, 457.
(32) Nieuwpoort, W. C.; Blasse, G. *Solid State Commun.* **1966**, *4*, 227.
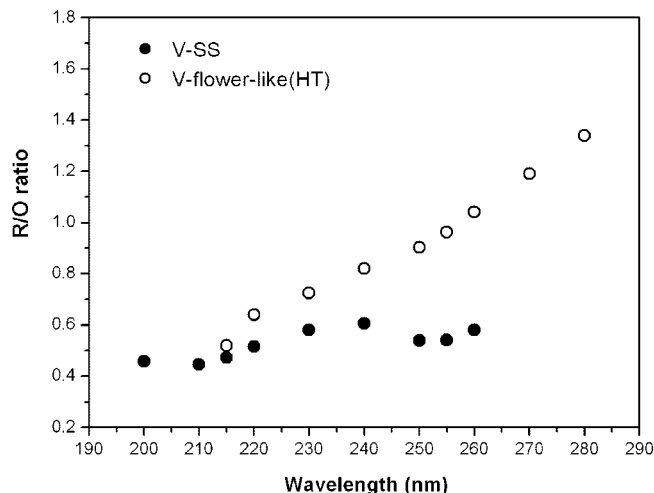
Figure 11. Ratio of red emission to orange emission of vaterite type LuBO$_3$: Eu^{3+} samples under excitation of UV lights with various wavelengths.

The interior Eu^{3+} and outside Eu^{3+} of V-flower-like(HT) sample present different luminescence properties as shown in Figures 9−11. It is well-known that on the surface of nanoscaled luminescent materials there are many defects acting as nonradiative luminescence quenchers. These quenchers provide the luminescence centers with many nonradiative relaxation paths, hence speeding up deexcitation of the excited luminescence centers, and shortening their fluorescence lifetimes. Considering the factor of distance between a luminescence center and a quencher at the surface, the outside Eu^{3+} can be strongly affected by the surface quenchers, and the interior Eu^{3+} can not. To test this assumption, the fluorescence decay curves monitoring at 610 nm of $^5D_0-^7F_2$ transition of Eu^{3+} are measured under nanosecond-pulsed laser excitation at 468 nm for the $^7F_0-^5D_2$ transition, or at 266 nm for the tail of CTB, as shown in Figure 12.

It is clearly demonstrated in V-flower-like(HT) sample that the fluorescence decays faster for 266 nm excitation than that for 468 nm excitation. The 266 nm excitation prefers the outside Eu^{3+} rather than the interior Eu^{3+} as shown in Figure 8, whereas the 468 nm excitation is a nonselective excitation to the outside and interior Eu^{3+} because of f−f transition. The nonlinear decay for the 266 nm excitation reflects the contribution from both the outside Eu^{3+} and interior Eu^{3+}. The decays for 468 nm excitation in both V-flower-like(HT) and V-SS exhibit a linear pattern with a time constant of about 2.69−2.88 ms. The emission spectrum upon 395 nm excitation in V-flower-like(HT), as shown in Figure 9, is the same as that in V-SS bulk sample, indicating that 395 nm excitation prefers selecting the interior Eu^{3+} at B type center in V-flower-like(HT). This implies that the interior Eu^{3+} ions dominate the luminescence even in the V-flower-like(HT) for f−f nonselective excitation. The reason for this result can be understood by the following analysis. On the one hand, the number of outside Eu^{3+} ions is much less than that of interior Eu^{3+} ions because the size of the substructures in V-flower-like(HT) is on the scale of 100 nm, not too small to have more sites near or on the surface. On the other hand, the outside Eu^{3+} ions have low luminescence efficiency because of surface quenchers. In
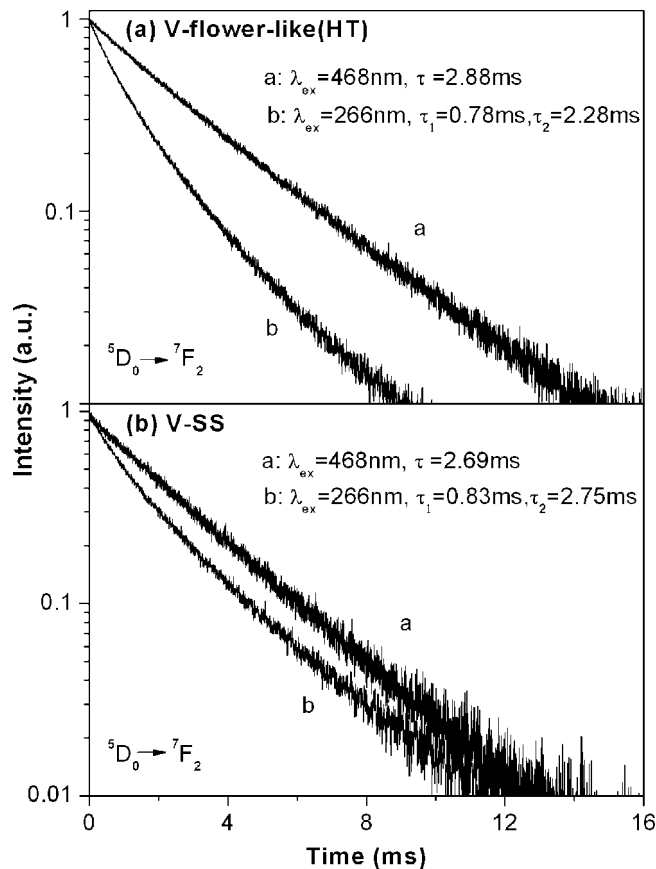
Figure 12. Fluorescence decay curves of $^5D_0-^7F_2$ transition of vaterite type LuBO$_3$:Eu^{3+} for (a) sample V-flower-like(HT) and (b) sample V-SS.

view of this consideration, it is reasonably understood that the luminescence is almost from the interior Eu^{3+} in the V-flower-like(HT) sample unless the outside Eu^{3+} is selectively excited, e.g., excitation at 266 nm. In the V-SS sample, the decays for both 266 and 468 nm excitation exhibit an approximate time constant. This result is easily understood considering the negligible surface effect for the V-SS bulk material, which has no nanoscaled substructures.

4. Conclusions

In conclusion, the calcite and vaterite type LuBO$_3$:Eu^{3+} nano/microcrystals were successfully synthesized by hydrothermal (HT) approach at 200−220 °C. In the HT synthetic process, the pH value of the precursor solution has a crucial effect on the formation of phase type and morphology of LuBO$_3$:Eu^{3+} samples. When the pH is adjusted to 7, a pure calcite type LuBO$_3$:Eu^{3+} with diamond morphology is formed; however, no product can be obtained if the pH is below 7. With gradually increasing the pH from 7, the vaterite phase in a shape of microclewlike appears and completely governs the products as the pH reaches to 8.7. The microclewlike products gradually change their shapes to be microflowerlike without crystal phase transformation as the pH value is further increased. The products are finally in the shape of microflowerlike when the pH is only 9.

The luminescence properties of these HT samples evidently show differences in comparison to that of the bulk powders prepared by the traditional solid-state (SS) reaction

method. The calcite type HT LuBO$_3$:Eu^{3+} presents a symmetrical and narrower CTB, It is considered to be the absence of O−Lu excitonic excitation due to exciton annihilation by the residual OH$^-$ groups introduced in HT synthesis. In the vaterite type LuBO$_3$:Eu^{3+}, there appear two Eu^{3+} centers, one with inversion symmetry. The HT sample with nanostructures such as vaterite type microflowerlike LuBO$_3$:Eu^{3+} demonstrates a red shift in the CTB and appearance of a long excitation tail at the long wavelength side of the CTB. The red shift is induced by an increase in crystal lattice parameters, and the long excitation tail is related to the Eu^{3+} ions located at lower symmetric sites. These sites are attributed to the outside Eu^{3+}. As the outside Eu^{3+} are selectively excited, the red emission of $^5D_0 - ^7F_2$ of Eu^{3+} enhanced relative to the orange emission of $^5D_0 - ^7F_1$, exhibiting superior color chromaticity in red for display application. The luminescence properties of LuBO$_3$:Eu^{3+} with nanostructures can be well-understood regarding Eu^{3+} ions as interior Eu^{3+} and outside Eu^{3+}.

CM802015U